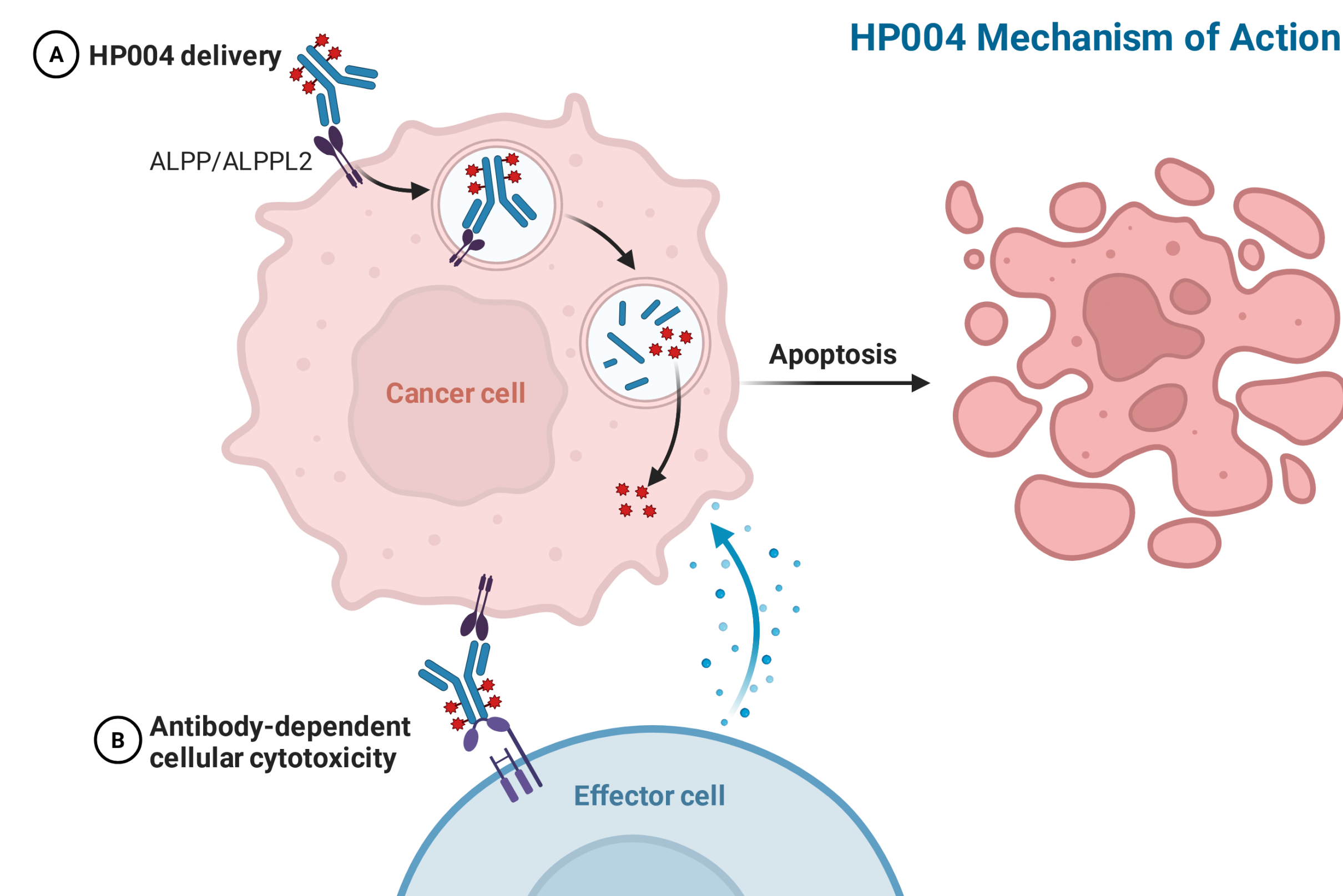


Abstract

Alkaline phosphatase placental (ALPP) and ALP-like 2 (ALPPL2) are highly expressed in a wide set of solid tumors, including ovarian, endometrial, gastric and non-small cell lung cancers. Their expression is highly restricted in normal tissues. ALPP/ALPPL2 are attractive targets for antibody-drug conjugate (ADC) and CAR-T therapies.

HP-004 is a novel ADC targeting both ALPP and ALPPL2, with high selectivity and enhanced internalization efficiency. HP-004 specifically binds ALPP/ALPPL2 but not the related isozymes ALPI or ALPL, minimizing potential on-target off-tumor liability. In cellular internalization assays using ALPP/ALPPL2 high- and low-expressing tumor cells, HP-004 demonstrated higher uptake and an improved capacity to deliver cytotoxic payload intracellularly across a range of target expression levels. HP-004 is site-specifically conjugated with monomethyl auristatin E (MMAE) with an average DAR about 4. In vitro, HP-004 induced potent target-dependent cytotoxicity in ALPP/ALPPL2-overexpressing tumor cell lines, with an IC₅₀ of approximately 248 pM. In the ALPP/ALPPL2-positive NCI-H1651 xenograft lung cancer model, HP-004 administration achieved near-complete tumor regression at 3 mg/kg (BiW X2), with complete tumor regression in 6 of 8 mice, demonstrating a robust antitumor activity. HP-004 is further being evaluated in cell line- and patient-derived xenograft models with different expression levels of ALPP and ALPPL2. In parallel, bispecific ADC formats incorporating HP-004 are being explored to further enhance therapeutic index and extend activity to heterogeneous or low-antigen tumors. Collectively, our data support HP-004 as a highly selective ADC candidate with superior internalization, strong preclinical efficacy, and promising potential for translation in solid tumors expressing ALPP/ALPPL2.

HP004 Mechanism of Action



HP004 is a human IgG1 antibody–drug conjugate (ADC) directed against ALPP/ALPPL2 that exerts its antitumor activity through both payload-mediated cytotoxicity and Fc-dependent effector functions.

After specific binding to ALPP/ALPPL2 on the surface of tumor cells, HP004 is internalized and trafficked to the endo-lysosomal compartment, where the linker is cleaved and the cytotoxic payload is released to induce intracellular damage (e.g., cell-cycle arrest and apoptosis), leading to potent, target-dependent tumor cell killing and potential bystander effects in antigen-low neighboring tumor cells.

In parallel, the intact IgG1 Fc region engages Fcγ receptors on NK cells and other effector cells, triggering antibody-dependent cell-mediated cytotoxicity (ADCC) and further amplifying tumor cell clearance beyond the direct ADC effect.

Together, these mechanisms provide dual killing via targeted payload delivery and immune-mediated cytotoxicity, aiming to achieve deep and durable tumor burden reduction in ALPP/ALPPL2-positive tumors.

ALPP/ALPPL2 Expression in Cancer

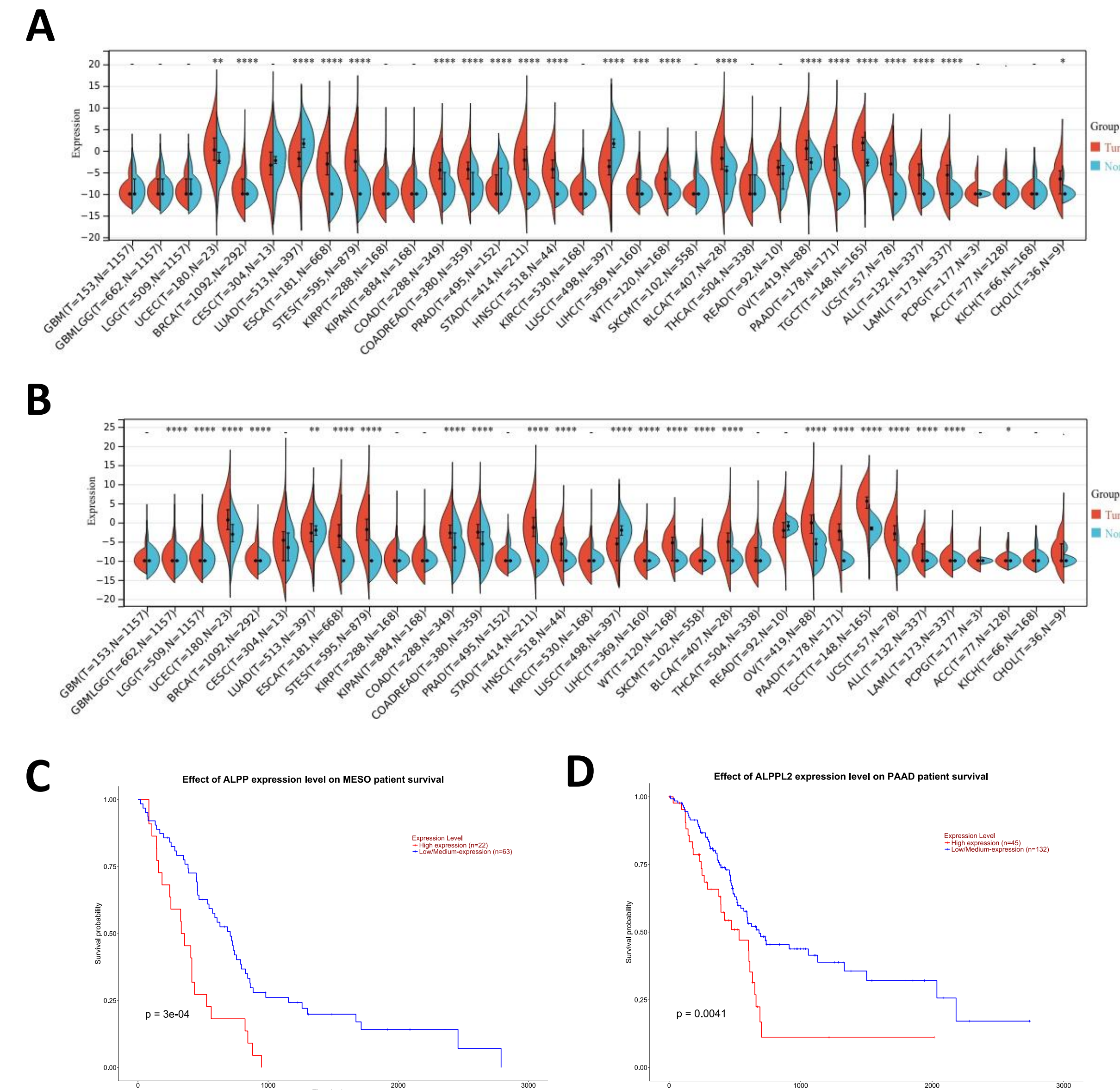


Figure 1: ALPP and ALPPL2 expression across tumor types and association with patient survival. (A–B) Differential expression of ALPP (A) and ALPPL2 (B) across multiple cancer types based on TCGA datasets, comparing tumor (red) versus normal (blue) tissues. Both ALPP and ALPPL2 show elevated expression in multiple tumor types relative to normal tissues. (C–D) Kaplan-Meier survival analyses demonstrates the association between gene expression and overall survival. High ALPP expression is associated with significantly poorer survival in mesothelioma (MESO) patients ($p = 3e-04$), while elevated ALPPL2 expression correlates with reduced survival in pancreatic adenocarcinoma (PAAD) patients ($p = 0.0041$).

Anti-ALPP/ALPPL2 Antibody Characterization for Binding, Internalization and Cytotoxicity

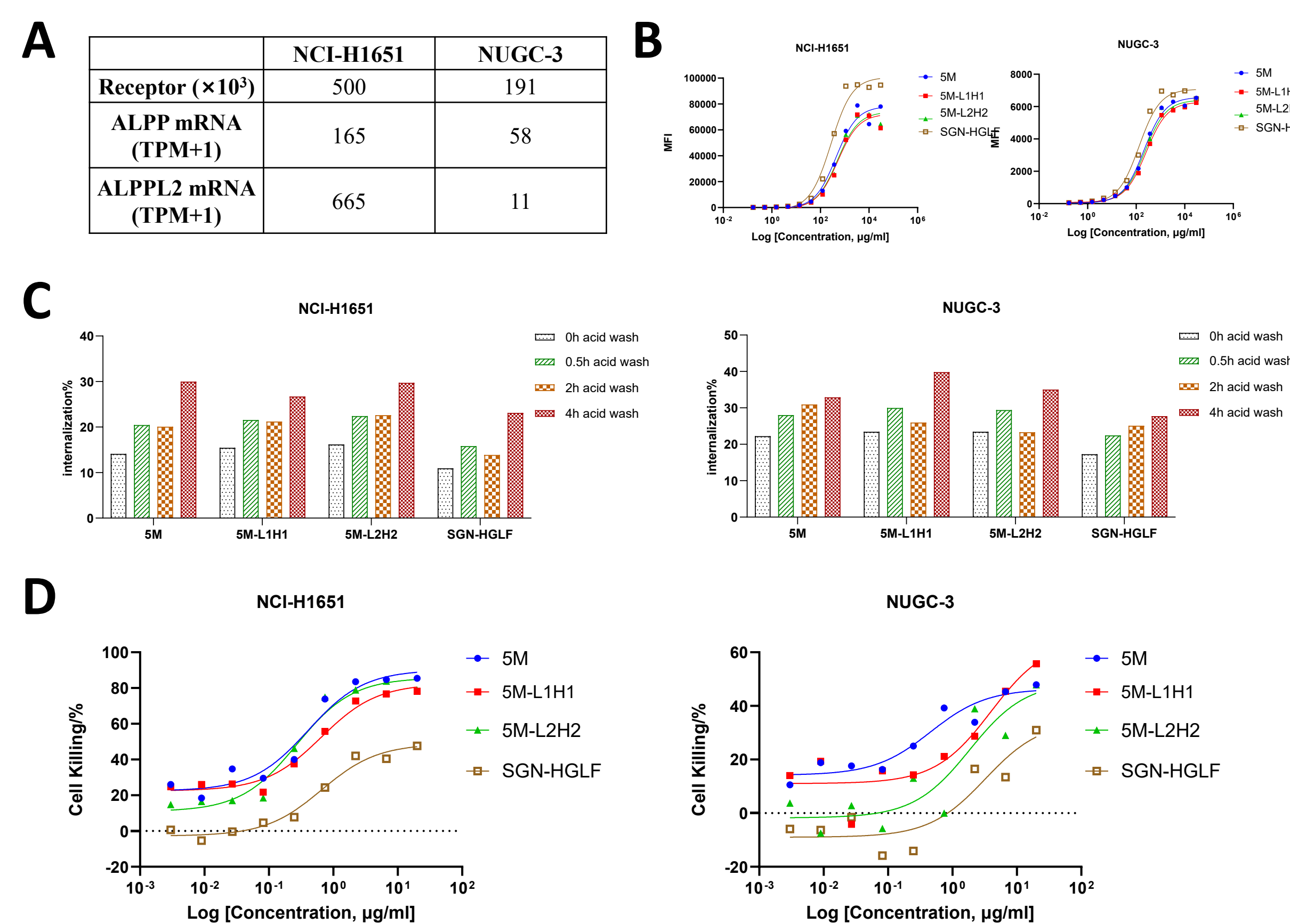


Figure 2: Comparison of antibody binding, internalization, and cytotoxic activity with SEAGEN reference antibody. **A.** Summary of ALPP, ALPPL2 expression on NCI-H1651 and NUGC-3 tumor cell lines. **B.** Binding activity of indicated antibodies measured by flow cytometry. Representative dose-response curves show mean fluorescence intensity (MFI) as a function of antibody concentration. **C.** Quantification of antibody internalization across different ALPP/ALPPL2 overexpressing tumor cells. Antibody internalization is presented as the percentage of internalized fraction under acid-wash conditions. **D.** In vitro cytotoxicity of antibodies evaluated using DT3C-mediated killing assays, with cell viability measured by CCK-8. Dose-response curves are shown as the percentage of cell killing versus log-transformed antibody concentration in two tumor cell models.

Antibody Engineering for ADC and RDC

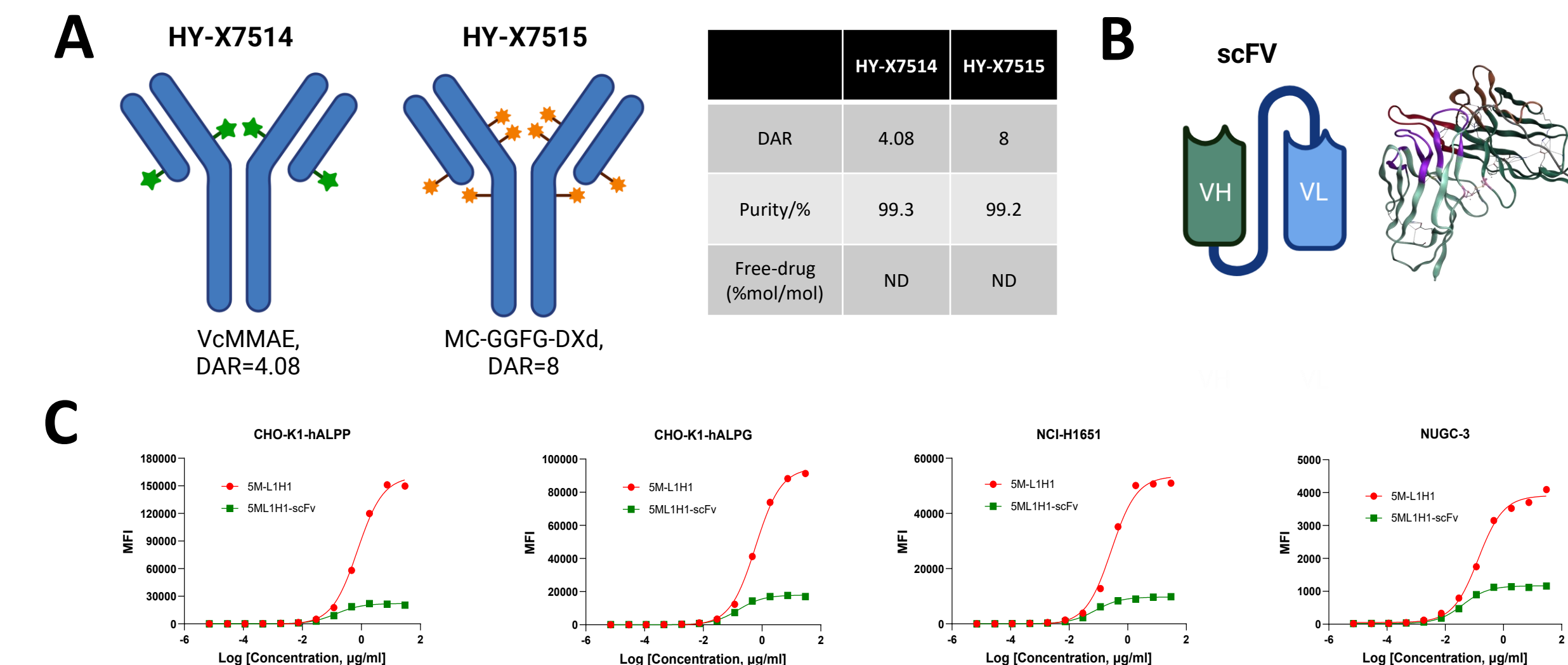


Figure 3: Characterization of HP004 antibody formats and binding properties. **A.** Schematic illustration of HP004 ADC constructs with different drug-to-antibody ratios (DAR). Conjugation profiles for HY-X7514 and HY-X7515 are shown, with corresponding DAR, purity, and free-drug levels summarized. **B.** Structural model of the HP004 scFV (VH–VL) generated by AlphaFold prediction, highlighting the overall folding and variable domain organization. **C.** Binding activity of the scFV format compared with the parental antibody, measured by flow cytometry. Representative dose–response curves (MFI vs. log concentration) are shown across engineered cell lines (CHO-K1-hALPP, CHO-K1-hALPPL2) and tumor cell lines (NCI-H1651, NUGC-3). The scFV retained target binding ability but exhibited reduced binding strength compared with the full-length antibody across all tested cell models.

HP004 ADC Binding to ALPP and ALPPL2 on Tumor Cells

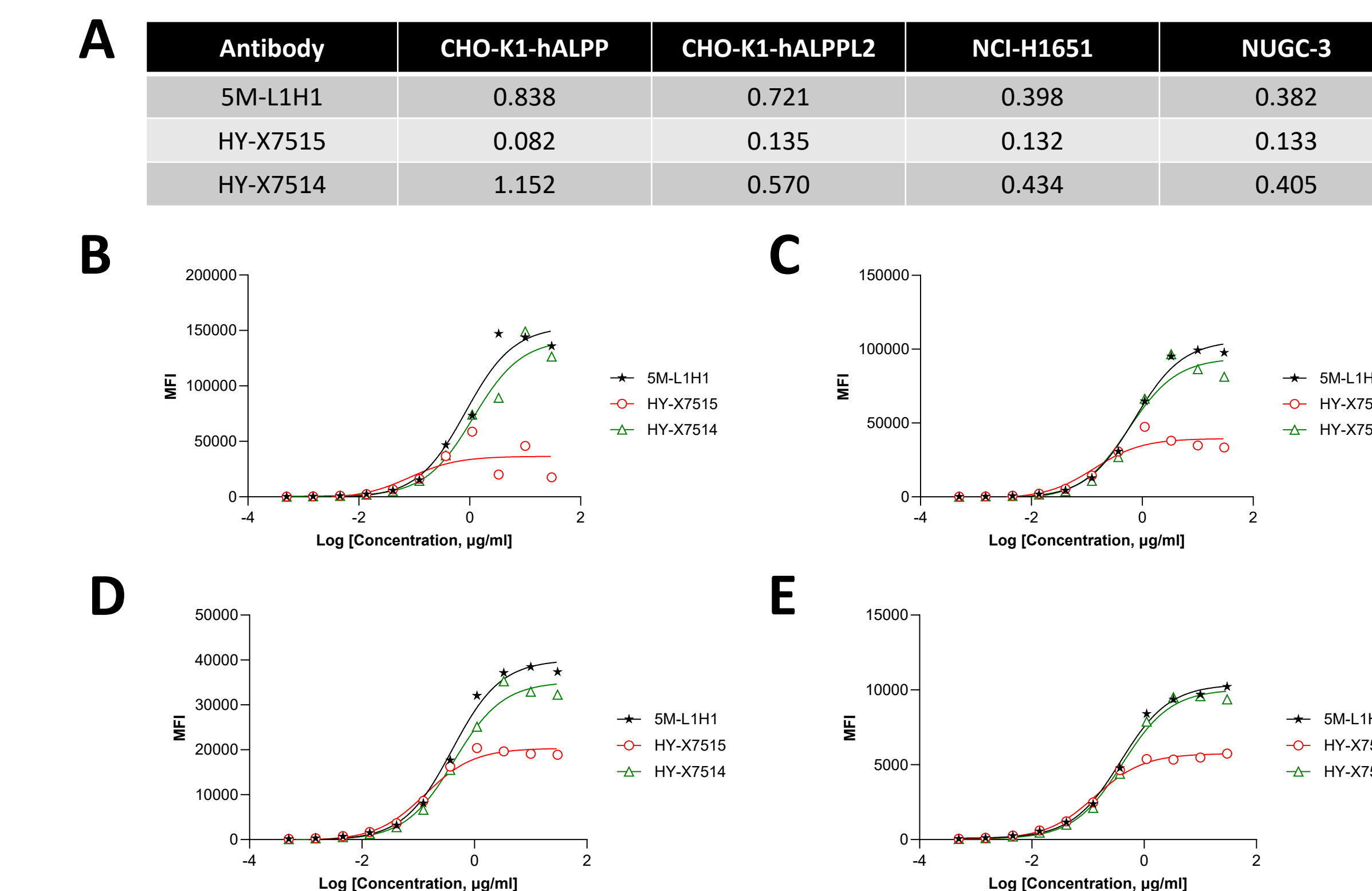


Figure 3: Binding of HP004 ADC to ALPP and ALPPL2 on tumor cells. **A.** Summary of binding (EC₅₀, ug/ml) of indicated antibodies to ALPP- and ALPPL2-expressing cells, including engineered CHO-K1-hALPP and CHO-K1-hALPPL2 cells, as well as tumor cell lines NCI-H1651 and NUGC-3. (B–E) Representative flow cytometry–based binding curves showing concentration-dependent binding of antibodies (SM-L1H1, HY-X7515, HY-X7514) to target-expressing cells. Data are presented as mean fluorescence intensity (MFI) versus log-transformed antibody concentration. (B) Binding to CHO-K1-hALPP cells. (C) Binding to CHO-K1-hALPPL2 cells. (D) Binding to NCI-H1651 cells. (E) Binding to NUGC-3 cells.

HP004 ADC Internalization into Tumor Cells Expressing ALPP and ALPPL2

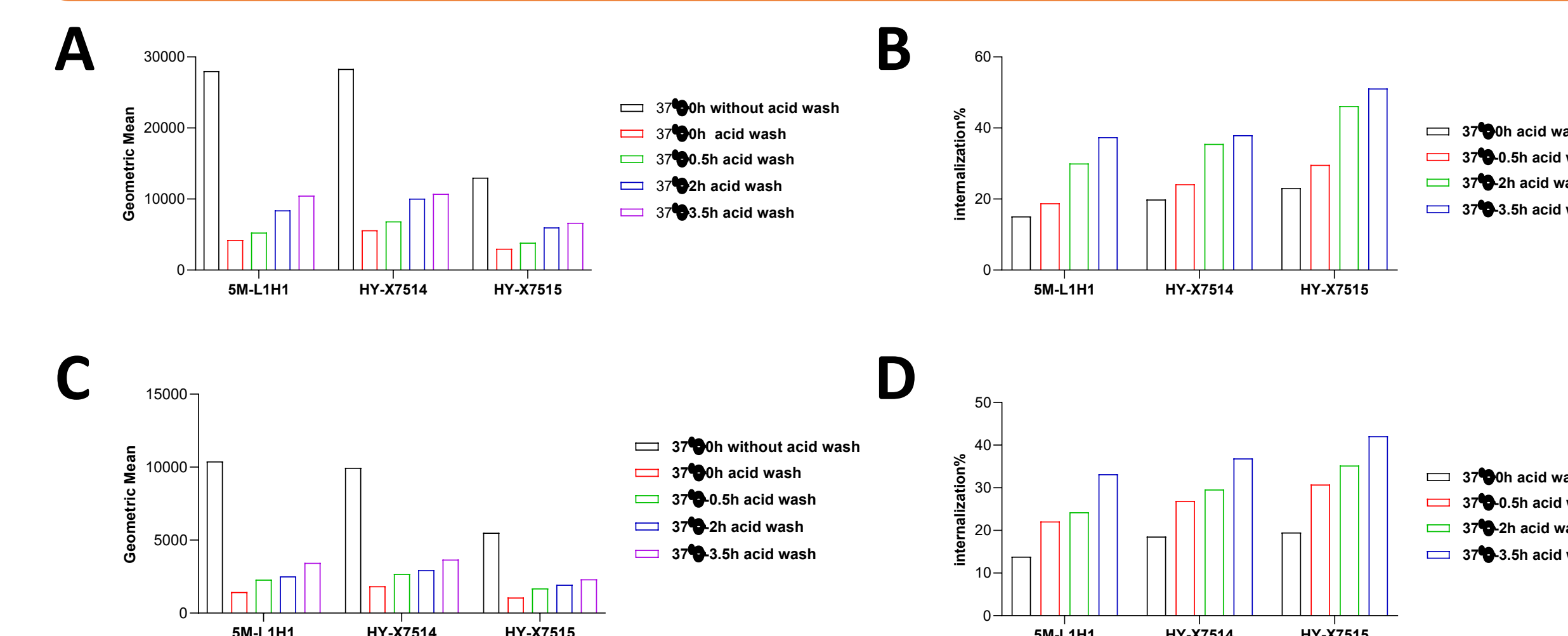


Figure 4: Efficient internalization of HP004 ADC in ALPP/ALPPL2-expressing tumor cells. (A, C) Quantification of cell-associated antibody signal (geometric mean fluorescence intensity, MFI) following incubation at 37 °C with or without acid wash. Acid wash removes surface-bound antibodies, allowing discrimination of internalized fractions over time (0, 0.5, 2, and 3.5 h). (B, D) Corresponding internalization percentages calculated from acid-wash conditions, demonstrating time-dependent increases in intracellular accumulation. (A–B) Internalization in NCI-H1651 tumor cells. (C–D) Internalization in NUGC-3 tumor cells.

HP004 *in vitro* Effectively Kills Tumor Cells Expressing ALPP/ALPPL2

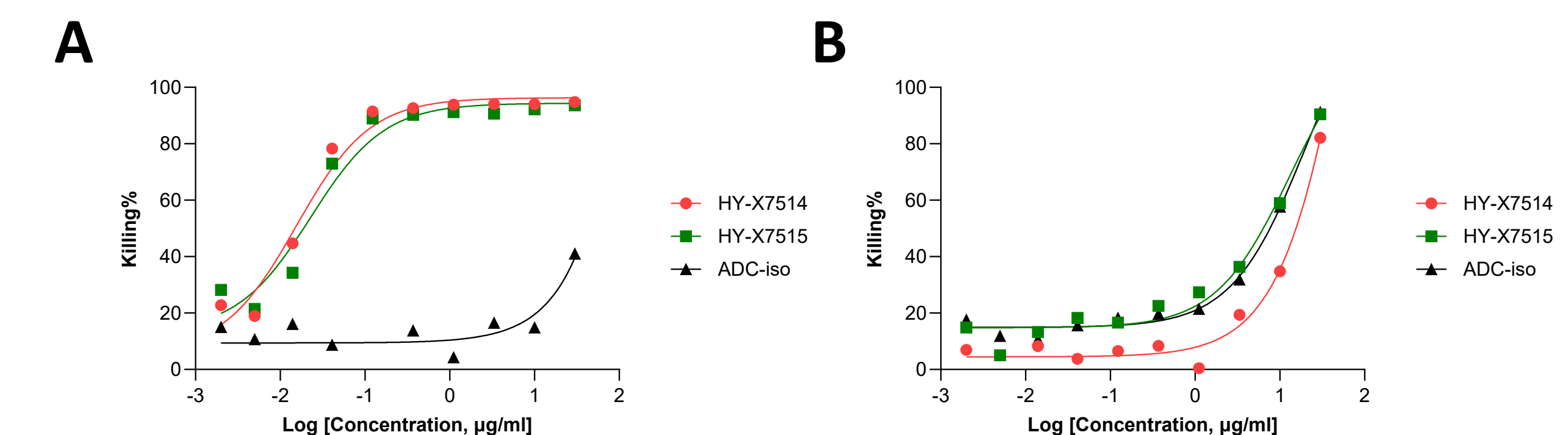


Figure 5: HP004 ADC-mediated cytotoxicity against ALPP- and ALPPL2-expressing tumor cells in vitro. In vitro cytotoxicity of HP004 ADC evaluated by CCK-8 assay following treatment with increasing concentrations of indicated antibodies (HY-X7514, HY-X7515) or isotype control ADC (ADC-iso). Cell killing is presented as the percentage of growth inhibition versus log-transformed antibody concentration. (A) Cytotoxic activity in NCI-H1651 tumor cells. (B) Cytotoxic activity in NUGC-3 tumor cells. HP004 ADC demonstrated potent and dose-dependent tumor cell killing in both models, whereas minimal cytotoxicity was observed with the isotype control ADC.

HP004 Bystander Killing Activity

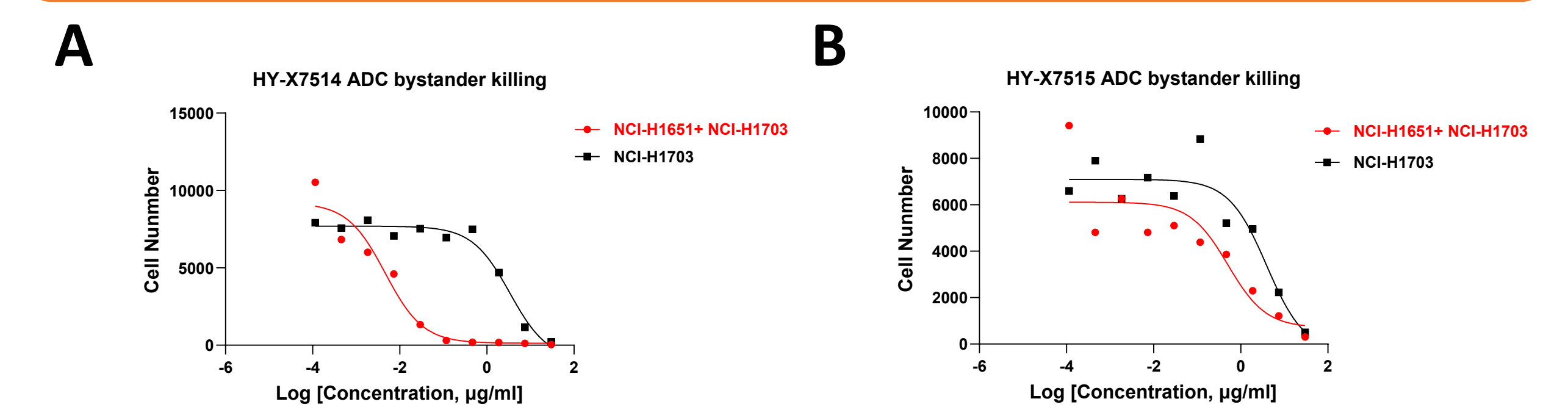


Figure 6: Bystander killing activity of HP004 ADC in co-culture tumor model. **A.** Bystander killing activity of HY-X7514 ADC (MMAE, DAR = 4.08) evaluated in a co-culture system of ALPP/ALPPL2-positive NCI-H1651 cells and antigen-negative NCI-H1703 cells. Cell viability was assessed following treatment with increasing ADC concentrations, and cell numbers are plotted against log-transformed concentration. HY-X7514 induced potent killing in the mixed-cell population (NCI-H1651 + NCI-H1703), while showing limited activity in NCI-H1703 monoculture, indicating a strong bystander effect. **B.** Bystander killing activity of HY-X7515 ADC (DXd, DAR = 8) assessed under the same conditions. Compared with HY-X7514, HY-X7515 demonstrated weaker bystander killing, with reduced potency in the co-culture model.

Robust *in vivo* Antitumor Efficacy of HP004

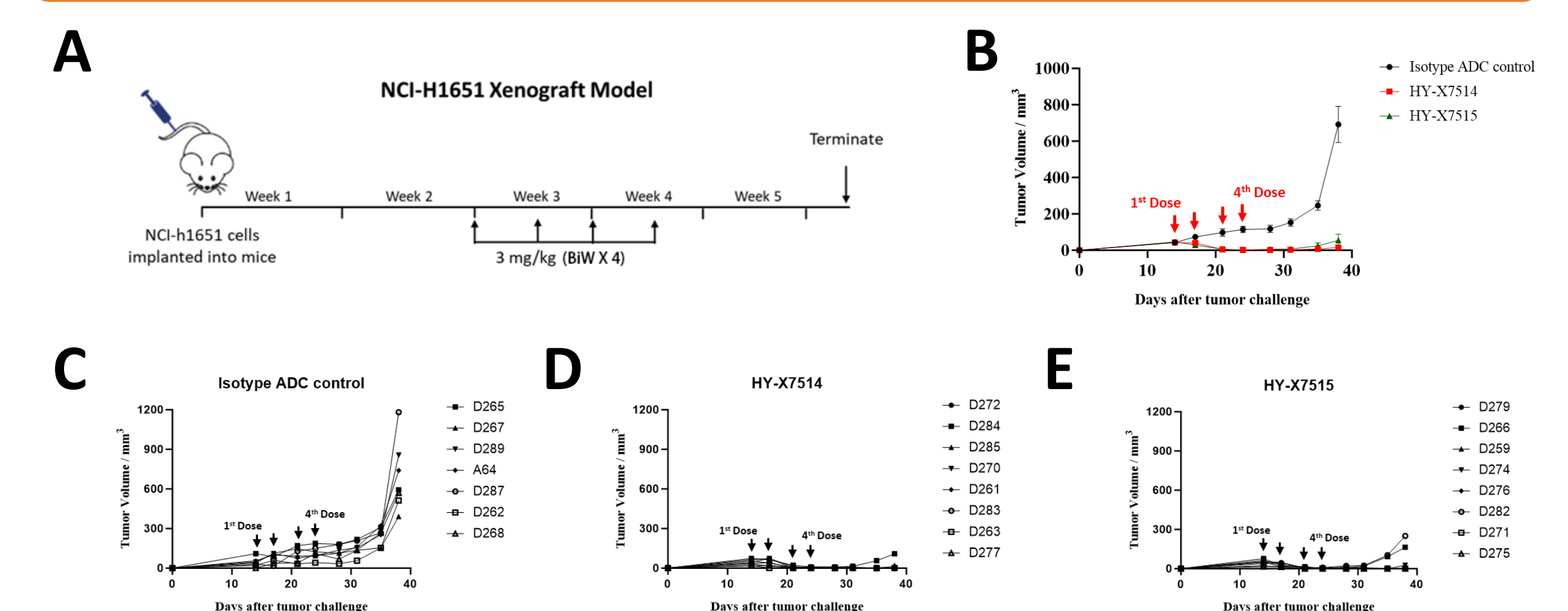


Figure 7: Robust *in vivo* antitumor efficacy of HP004. **A.** Schematic representation of the *in vivo* efficacy study design. Tumor-bearing mice were treated with HP004 via repeated dosing as indicated (arrows). Tumor growth was monitored over time and compared with control treatment. **B.** Tumor growth kinetics following HP004 treatment. Arrows indicate dosing time points. HP004 treatment resulted in sustained tumor growth inhibition compared with the control, with divergence observed following repeated dosing. (C–E) Tumor growth curves for individual mice in different treatment groups, demonstrating consistent and reproducible tumor suppression across treated animals compared with the control ADC.

Summary

HP004 are human IgG1 antibody–drug conjugates (ADCs) directed against ALPP/ALPPL2 that exert antitumor activity through both payload-mediated cytotoxicity and Fc-dependent effector functions.

HP004's anti-ALPP/ALPPL2 antibody has improved internalization efficiency and cytotoxic activity compared with SGN reference antibody.

HY-X7514 is conjugated with MMAE with an average DAR about 4. HY-X7515 is conjugated with DXd with an average DAR about 8. Both ADC candidates demonstrated potent target-dependent cytotoxicity *in vitro* and consistent anti-tumor efficacy *in vivo*. Both HY-X7514 and HY-X7515 led to sustained tumor growth inhibition in xenograft tumor models.